A systematic examination of the relationships between CDOM and DOC in inland waters in China

Kaishan Song[1], Ying Zhao[1, 2], Zhidan Wen[1], Chong Fang[1, 2], Yingxin Shang[1]

[1]Northeast Institute of Geography and Agroecology, CAS, Changchun, 130102, China

[2] University of Chinese Academy of Sciences, Beijing 100049, China

Corresponding author's E-mail: songks@iga.ac.cn; Tel: 86-431-85542364

Abstract: Chromophoric dissolved organic matter (CDOM) plays a vital role in the biogeochemical cycle in aquatic ecosystems. The relationship between CDOM and dissolved organic carbon (DOC) has been investigated, and the significant relationship lays the foundation for the estimation of DOC using remotely sensed imagery data. The current study examined the samples from freshwater lakes, saline lakes, rivers and streams, urban water bodies, and ice-covered lakes in China for tracking the variation of the relationships between DOC and CDOM. The regression model slopes for DOC versus $a_{CDOM}(275)$ ranged from extreme low 0.33 (highly saline lakes) to 1.03 (urban waters) and 3.01 (river waters). The low values were observed in saline lake waters and waters from semi-arid or arid regions where strong photo-bleaching is expected due to thin ozone layers, less cloud cover, longer water residence time and daylight hours. In contrast, high values were found in waters developed in wetlands or forest in Northeast China, where more organic matter was transported from catchment to waters. The study also demonstrated that stronger relationships between CDOM and DOC were revealed when $a_{CDOM}(275)$ were sorted by the ratio of $a_{CDOM}(250)/a_{CDOM}(365)$, which is a tracer

for the CDOM absorption with respect to its composition, and the determination of coefficient of the regression models ranged from 0.75 to 0.98 for different groups of waters. Our results indicated the relationships between CDOM and DOC are variable for different inland waters, thus models for DOC estimation through linking with CDOM absorption need to be tailored according to water types.

Keywords: Absorption, CDOM, DOC, regression slope, saline water, fresh water

1. Introduction

Inland waters play a disproportional role for the global carbon cycling with respect to carbon transportation, transformation and carbon storage (Tranvik et al., 2009; Raymond et al., 2013; Verpoorter et al., 2014; Yang et al., 2015). However, the amount of dissolved organic carbon (DOC) stored in the inland waters is still unclear or the uncertainty is still needed to be evaluated (Tranvik et al., 2009). Determination DOC concentration is straightforward through field sampling and laboratory analysis (Findlay and Sinsabaugh, 2003). However, there are millions of lakes in the world, and many of them are remote and inaccessible, making it impossible to evaluate DOC concentration using routine approach (Cardille et al., 2013; Brezonik et al., 2015; Pekel et al., 2016). Researchers have found that remote sensing might provide a promising tool for quantification of DOC of inland waters at large scale through linking DOC with chromophoric dissolved organic matter (CDOM), particularly for inland waters situating in remote area with less accessibility (Tranvik et al., 2009; Kutser et al., 2015; Brezonik et al., 2015).

As one of the optically active constituents (OACs) in waters, CDOM can be estimated through remotely sensed signals (Yu et al., 2010; Kutser et al., 2015), and is acted as a proxy in many regions for the amount of DOC in the water column. As shown in Fig.1, CDOM and DOC in the aquatic ecosystems are mainly originated from external (allochthonous) and internal (autochthonous) sources, in addition to directly discharge from anthropogenic activities (Zhou et al., 2016). Generally, the autochthonous CDOM is essentially originated from algae and macrophytes, and

53 mainly consists of various compounds of low molecular weights (Findlay and
54 Sinsabaugh, 2003; Zhang et al., 2010). While, the allochthonous CDOM is mainly
55 derived from the surrounding terrestrial ecosystems, and it comprises a continuum of
56 small organic molecules to highly polymeric humic substances. In terms of CDOM
57 originates from anthropogenic, it contains fatty acid, amino acid and sugar, thus the
58 composition of CDOM is more complex than that from natural systems (Zhou et al.,
59 2016; Zhao et al., 2016a). Hydrological factors also affect the DOC and CDOM
60 characteristic and particularly, the discharge and catchment area are the important ones
61 (Neff et al., 2006; Spencer et al., 2012).

62 **[Insert Fig.1 about here]**

63 CDOM is a light-absorbing constituent, which is partially responsible for the color
64 in waters (Bricaud et al., 1981; Reche et al., 1999; Babin et al., 2003). The chemical
65 structure and origin of CDOM can be characterized by its absorption coefficients
66 ($a_{CDOM}(\lambda)$) and spectral slopes (De Haan and De Boer, 1987; Helms et al., 2008).
67 Weishaar et al. (2003) has proven that the carbon specific absorption coefficient at 254
68 nm, e.g., $SUVA_{254}$ is a good tracer for the aromaticity of humic acid in CDOM, while
69 the ratio of CDOM absorption at 250 to 365 nm, i.e., $a_{CDOM}(250)/a_{CDOM}(365)$, herein,
70 M value, has been successfully used to track the changes in DOM molecular weight
71 (De Haan and De Boer, 1987). Biodegradation and photodegradation are the major
72 processes to determine the transformation and composition of CDOM (Findlay and
73 Sinsabaugh, 2003; Zhang et al., 2010), which ultimately affect the relationship between
74 DOC and CDOM (Spencer et al., 2012; Yu et al., 2016). With prolonged sunlight

radiation, some of the colored fraction of CDOM is lost by the photobleaching processes (Miller et al., 1995; Zhang et al., 2010), which can be measured by the light absorbance decreasing at some specific (diagnostic) wavelength, e.g., 250, 254, 275, 295, 360 and 440 nm.

It should be noted that $a_{CDOM}(440)$ is usually used by remote sensing community due to this wavelength is overlapped with pigment absorption at 443 nm, thus reporting $a_{CDOM}(440)$ has potential to improve chlorophyll-a estimation accuracy (Lee et al., 2002). Under this circumstance, the relationship between CDOM and DOC varies since CDOM loses color while the variation of DOC concentration is almost negligible. Saline or brackish lakes in the arid or semi-arid regions generally expose to longer sunlight radiation, thus CDOM absorbance decreases, while DOC is accumulated due to the longer residence time (Curtis and Adams, 1995; Song et al., 2013; Wen et al., 2016). Compared to photodegradation on CDOM, the biodegradation processes by microbes are much complicated, and extracellular enzymes are the key substance required to decompose the high-molecular-weight CDOM into low-molecular-weight substrates (Findlay and Sinsabaugh, 2003). With compositional change, the absorption feature of CDOM and its relation to DOC varies correspondingly, but the relationship between CDOM and DOC is far from solved (Gonnelli et al., 2013). In addition, the $SUVA_{254}$ and M value may be used to classify CDOM into different groups and enhance the relationship with DOC based on CDOM absorption grouping.

Some studies have investigated the spatial and seasonal variations of CDOM and DOC in ice free season in lakes, rivers and oceans (Vodacek et al., 1997; Neff et al.,

2006; Stedmon et al., 2011; Brezonik et al., 2015), but less is known about saline lakes (Song et al., 2013; Wen et al., 2016). Even less is known about urban waters influenced by sewage effluent and waters with ice cover in winter (Belzile et al., 2002; Zhao et al., 2016b). The significant relationship between CDOM and DOC was observed in the Gulf of Mexico, and stable regression model was established between DOC and $a_{CDOM}(275)$ and $a_{CDOM}(295)$ (Fichot and Benner, 2011). Similar results were also found in other estuaries along a salinity gradient, for example the Baltic Sea surface water (Kowalczuk et al., 2010) and the Chesapeake Bay (Le et al., 2013). However, Chen et al. (2004) found that the relationship between CDOM and DOC was not conservative due to estuarine mixing or photo-degradation. Similar arguments were raised for Congo River and waters across mainland USA (Spencer et al., 2009, 2012). However, seasonal variations were observed in some studies due to the mixing of various endmembers of CDOM from different terrestrial ecosystems and internal source (Zhang et al., 2010; Spencer et al., 2012; Yu et al., 2016; Zhou et al., 2016).

In this study, the characteristics of DOC and CDOM in different inland waters across China were examined to determine the spatial feature associated with landscape variations, hydrologic conditions and saline gradients. The objectives of this study are to: 1) examine the relationship between CDOM and DOC concentrations across a wide range of waters with various physical, chemical and biological conditions, and 2) develop a model for the relationship between DOC and CDOM based on the sorted CDOM absorption feature, e.g., the M value with aiming to improve the regression modeling accuracy.

2. Materials and Methods

The dataset is composed of five subsets of samples collected from various types of waters across China (Table 1, Fig.2), which encompassed a wide range of DOC and CDOM. The first dataset (n = 288; from early spring 2009 to late October 2014) includes samples collected in freshwater lakes and reservoirs during the growing season with various landscape types. The second dataset (n = 345; from early spring 2010 to late mid-September 2014) includes samples collected in brackish to saline water bodies. The third dataset (n =322; from early May 2012 to late October 2014) includes samples collected in rivers and streams across different basins in China. In addition, 69 samples were collected from three sections along the Songhua Rive, the Yalu and the Hunjiang River during the ice free period in 2015 to examine the impact of river flow on the relationship between DOC and CDOM (see Fig.S1 for location). The fourth dataset (n = 328; from 2011 to 2014 in the ice frozen season) includes samples collected in Northeast China in winter from both lake ice and underlying waters. The fifth dataset (n = 221; from early May 2013 to mid-October 2014) collects samples in urban water bodies, including lakes, ponds, rivers and streams, which were severely polluted by sewage effluents. City maps and Landsat imagery data acquired in 2014 or 2015 were used to delineate urban boundaries with ArcGIS 10.0 (ESRI Inc., Redlands, California, USA), and water bodies in these investigated cities constrained by urban boundaries were considered as urban water bodies. Except river samples, the sampling dates, water body names and locations of other types of water bodies were provided in supplementary Table S1-3.

[Insert Fig.2 about here]

2.1 Water quality determination

Water samples were collected approximately 0.5m below the water surface at each station, generally locating in the middle of water bodies. Water samples were collected in two 1 L amber HDPE bottles, and kept in coolers with ice packs in the field and kept in refrigerator at 4℃ after shipping back to the laboratory. All samples were preprocessed (e.g., filtration, pH and electrical conductivity (EC) determination) within two days in the laboratory. Water salinity was measured using DDS-307 EC meter (μS/cm) at room temperature (20±2℃) and converted to *in situ* salinity, expressed in practical salinity units (PSU), in the laboratory. Water samples were filtered using Whatman cellulose acetone filter with pore size of 0.45 μm. Chlorophyll-a (Chl-a) was extracted and concentration was measured using a Shimadzu UV-2600PC spectrophotometer, the details can be found in Jeffrey and Humphrey (1975). Total suspended matter (TSM) was determined gravimetrically using pre-combusted Whatman GF/F filters with 0.7μm pore size, details can be found in Song et al. (2013). DOC concentrations were measured by high temperature combustion (HTC) with water samples filtered through 0.45 μm Whatman cellulose acetone filters (Zhao et al., 2016a). The standards for dissolved total carbon (DTC) were prepared from reagent grade potassium hydrogen phthalate in ultra-pure water, while dissolved inorganic carbon (DIC) were determined using a mixture of anhydrous sodium carbonate and sodium hydrogen carbonate. DOC was calculated by subtracting DIC from DTC, both of which were measured using a Total Organic Carbon Analyzer (TOC-VCPN, Shimadzu, Japan).

Total nitrogen (TN) was measured based on the absorption levels at 146 nm of water samples decomposed with alkaline potassium peroxydisulfate. Total phosphorus (TP) was determined using the molybdenum blue method after the samples were digested with potassium peroxydisulfate (APHA, 1998). pH was measured using a PHS-3C pH meter at room temperature (20±2℃).

2.2 CDOM absorption measurement

All water samples were filtered at low pressure at two steps: 1) filtered at low pressure through a pre-combusted Whatman GF/F filter (0.7μm), and 2) further filtered through pre-rinsed 25 mm Millipore membrane cellulose filter (0.22 μm). Absorption spectra were obtained between 200 and 800 nm at 1 nm increment using a Shimadzu UV-2600PC UV-Vis dual beam spectrophotometer (Shimadzu Inc., Japan) through a 1 cm quartz cuvette (or 5 cm cuvette for ice melted water samples). Milli-Q water was used as reference for CDOM absorption measurements. The Napierian absorption coefficient (a_{CDOM}) was calculated from the measured optical density (*OD*) of samples using Eq. (1):

$$a_{CDOM}(\lambda) = 2.303[OD_{S(\lambda)} - OD_{(null)}] / \beta \quad (1)$$

where β is the cuvette path length (0.01 or 0.05m) and 2.303 is the conversion factor of base 10 to base *e* logarithms. To remove the scattering effect from the limited fine particles remained in the filtered solutions, a necessitated correction was implemented by assuming the average optical density over 740–750 nm to be zero (Babin et al., 2003). $SUVA_{254}$ and M values were calculated to characterize CDOM with respect to their compositional features. In addition, a_{CDOM} was divided into different groups according

to M values by hierarchical cluster approach, which was performed in SPSS software package with the pairwise distance between samples was measured by squared Euclidean distance and the clusters were linked together by Ward's linkage method (Ward Jr, 1963). The method has been applied to classify the waters into different types according the remote sensing spectra (Vantrepotte et al., 2012; Shi et al., 2013).

3. Results

3.1. Water quality characteristics

Chl-a concentrations (46.44±59.71 μg/L) changed from 0.28 to 521.12μg/L. TN and TP concentrations were very high in fresh lakes, saline lakes and particularly urban water bodies (Table 1). It is worth noting that Chl-a concentration was still high 7.3±19.7μg/L even in ice-covered lakes in winter from Northeast China. Electric conductivity (EC) and pH were high in the semi-arid and arid regions, and they were 1067-41000 μs/cm and 7.1-11.4, respectively. Overall, waters were highly turbid with high TSM concentrations (119.55 ± 131.37 mg/L), and apparent variations were observed for different types of waters (Table 1). Hydrographic conditions exerted strong impact on water turbidity and TSM concentration, thus these two parameters of river and stream samples were excluded in this study (Table 1).

[Insert Table 1 about here]

3.2. DOC concentrations in different types of waters

DOC concentrations changed remarkably in the investigated waters (Table 1). DOC concentrations were low in rivers, while they were much lower in ice melting waters sampled in winter. It should be noted that large variations were observed in water

samples from rivers and streams (Table 2). Among the five types of waters, relatively higher DOC concentrations, ranging from 2.3 to 300.6 mg/L, were found in many saline lakes, in the Songnen Plain, the HulunBuir Plateau and some areas in Tibetan Plateau (see Fig.2 for location). However, some of saline lakes supplied by snow melt water or ground water exhibited relatively lower DOC concentrations even with high salinity. Compared with samples collected in growing seasons, higher DOC concentrations (7.3-720 mg/L) were observed in ice-covered water bodies.

[Insert Table 2 about here]

3.3. DOC versus CDOM for various types of waters

3.3.1 Freshwater lakes and reservoirs

The relationship between DOC and CDOM has been investigated based on CDOM absorption spectra at different wavelengths (Fichot and Benner, 2011; Spencer et al., 2012; Song et al., 2013; Brezonik et al., 2015). As suggested by Fichot and Benner (2011), CDOM absorptions at 275 nm ($a_{CDOM}(275)$) and 295 nm ($a_{CDOM}(295)$) have stable performances for DOC estimates for coastal waters. In current study, a strong relationship ($R^2 = 0.85$) between DOC and $a_{CDOM}(275)$ was found in fresh lakes and reservoirs (Fig.3a). However, the participation of $a_{CDOM}(295)$ explains very limited variance, thus it is not considered in the regression models. Regression analyses of water samples collected from different regions indicated that the slopes varied from 1.30 to 3.01 (Table 3). Water samples collected from East China and South China had lower regression slope values (Table 3), and lakes and reservoirs were generally mesotrophic or eutrophic (Huang et al., 2014; Yang et al., 2012, and references therein).

[Insert Table 3 about here]

[Insert Fig.3 about here]

3.3.2 Saline lakes

A strong relationship between DOC and $a_{CDOM}(275)$ ($R^2 = 0.85$) was demonstrated for saline lakes (Fig.3b). Much lower regression slope value (slope = 1.28) was found in saline lakes. Similar to fresh waters, the slopes of most saline lakes exhibited large variations between different regions (Table 3), ranging from 0.86 in Tibetan waters to 2.83 in the Songnen Plain waters (see Fig.2 for location). As the extreme case, the slope value was only 0.33 as demonstrated in the embedded diagram in Fig.3b. Saline lakes in semi-arid or arid regions generally exhibit higher regression slope values, for example, the west Songnen Plain (2.83), the Hulunbir Plateau and the East Inner Mongolia Plateau (1.79). Whereas, waters in the west Inner Mongolia Plateau (1.13), the Tibetan Plateau (0.86) exhibited low slope values (Table 3), and the extreme low value was measured in the Lake Qinhai in Tibetan Plateau. Lakes in Tarim Basin were affected by strong photo-bleaching, due to the long resident time and strong solar radiation (Spencer et al., 2012; Song et al., 2013; Wen et al., 2016).

3.3.3 Streams and rivers

Although some of the samples scattered from the regression line (Fig.3c), close relationship between DOC and $a_{CDOM}(275)$ was found for samples collected in rivers and streams. Compared with the other water types (Fig.3), rivers and streams exhibited the highest regression slope value (slope = 3.01). Further regression analysis with water samples sub-datasets collected in different regions indicated that slope values presented

large variability, ranging from 1.07 to 8.49. The lower regression slope values were recorded in water samples collected in rivers and stream in semi-arid and arid regions, such as the Tibetan Plateau, Mongolia Plateau and Tarim Basin, while the higher values were found in samples collected in streams originated from wetland and forest in Northeast China (Table 3).

To investigate the dynamics of CDOM absorption and DOC concentrations, three sections were investigated in three major rivers in Northeast China (see Figure S1 for location). River flow exerted obvious effect on DOC and CDOM (Fig.4) and flood impulse brought large amount of DOC and CDOM into river channels. The relationships between DOC and $a_{CDOM}(275)$ in sections along three rivers in Northeast China were demonstrated in Fig.5. The sampling point in the Yalu River is near the river head source, thus strong relationship was exhibited with large slope (Fig.5a). The relationship between DOC and $a_{CDOM}(275)$ in the Songhua River at Harbin City section was much scattered (Fig.5c). With respect to Fig.5b, it is an in-between case. The sampling point was affected by effluent from Baishan City, thus the coefficient of determination (R^2= 0.822) and the regression slope (3.72) were lower than that from the Yalu River at Changbai point, while higher than that from the Songhua River at Harbin point.

[Insert Fig.4 and Fig.5 about here]

3.3.4 Urban waters

Relative close relationship between DOC and $a_{CDOM}(275)$ was revealed in urban waters (Fig.3d, R^2= 0.71). Similarly, regression slope values changed remarkably, ranging

from 0.87 to 2.45. High nutrients also usually result in algal bloom in most urban water bodies (Chl-a range: 1.0-521.1μg/L; average: 38.9μg/L). Thereby, DOC and CDOM derived from phytoplankton may also contribute a portion that should not be neglected (Zhang et al., 2010; Zhao et al., 2016b; Zhou et al., 2016).

3.3.5 Ice covered lakes and reservoirs

The closest relationship (R^2 = 0.93) between DOC and $a_{CDOM}(275)$ was recorded in waters beneath ice covered lakes and reservoirs in Northeast China (Fig.3e). Comparatively, a weak relationship between DOC and $a_{CDOM}(275)$ was demonstrated in ice melting waters (Fig.3f). Apparently, CDOM from ice melting waters were mainly originated from maternal water during the ice formation, also from algal biological processes (Stedmon et al., 2011; Arrigo et al., 2010). Interestingly, the regression slopes for ice samples (1.35) and under lying water sample (1.27) are very close. In addition, there was a significant relationship between DOC in ice and underlying waters (R^2 = 0.86), indicating the dominant components of CDOM and DOC in the ice are from maternal underlying waters.

3.3.6 DOC versus $a_{CDOM}(440)$

CDOM absorption at 440 nm, i.e., $a_{CDOM}(440)$, is usually used as a surrogate to represent its concentration (Bricaud et al., 1981; Babin et al., 2003), and widely used in remote sensing community to quantify CDOM in waters (Lee et al., 2002; Binding et al., 2008; Zhu et al., 2014). Significant relationships between DOC and $a_{CDOM}(440)$ were found in different types of waters (Fig.5). Through comparing Fig.3 with Fig.6, it can be found that the overall relationships between DOC and CDOM at 440 nm

295 resembled that at 275 nm for different types of waters.

296 **[Insert Fig.6 about here]**

297 **3.4 CDOM molecular weight and aromacity versus DOC**

298 ***3.4.1 CDOM versus $SUVA_{254}$ and M value ($a_{CDOM}(250)/a_{CDOM}(365)$)***

299 The large slope variations of regressions between DOC and $a_{CDOM}(275)$ in different
300 types of waters are probably due to the aromacity and colored fractions in DOC
301 component (Spencer et al., 2009, 2012; Lee et al., 2015). As shown in Fig.7a, it can be
302 seen that $SUVA_{254}$ had high values in fresh lakes, and waters from rivers or streams as
303 well. Saline water and ice covered waters in Northeast China showed intermediate
304 $SUVA_{254}$ values, while urban water and ice melting water exhibited lower values. The
305 M value, i.e., $a_{CDOM}(250)/a_{CDOM}(365)$ is another indicator to demonstrate the variation
306 of molecular weight of CDOM components (De Haan, 1993). Compared to saline
307 waters, fresh lake water (*t-Test*, $F = 631$, $p < 0.001$), river and stream water ($F = 547$, p
308 < 0.001), and urban water ($F = 396$, $p < 0.001$) exhibited low M values (Fig.7b), which
309 indicated that large weight molecules dominate in these three types of waters. Saline
310 water, ice covered water in Northeast China and ice melting water showed higher M
311 values. Since $SUVA_{254}$ is a proxy based on the ratio to DOC, it is inappropriate to
312 establish the relationship between CDOM and DOC based on the $SUVA_{254}$
313 classification. Thereby, only M values, which reveal molecular weight and aromacity,
314 might help to estimate DOC through CDOM absorption based on M values for various
315 types of waters.

316 **[Insert Fig.7 about here]**

317 ***3.4.2 Regression based on M values***

318 Regression models between DOC and $a_{CDOM}(275)$ were established based on M value
319 grouping. Four groups were achieved with hierarchical cluster approach, and each
320 group occupied about 43.48% (M < 8.5), 34.38% (8.5< M < 16.1), 19.35% (16.1< M <
321 25.6) and 2.79% (25.6< M < 68.0) of the total samples from group 1 to 4, respectively.
322 Though only M values were used in the cluster which meant the feature space in
323 classification only had one dimension and the groups were mainly divided according to
324 the distribution of M values, the hierarchical cluster approach generated rational results.
325 A close relationship ($R^2 = 0.92$) between DOC and $a_{CDOM}(275)$ was revealed in dataset
326 where M < 8.5 (Fig.8a). Likewise, close relationship regression model appeared in
327 dataset with intermediate M values (Fig.8b), revealing high determination of
328 coefficients ($R^2 = 0.93$). As shown in Fig.8c, a relative weak relationship ($R^2 = 0.75$)
329 between DOC and $a_{CDOM}(275)$ appeared with M values ranging from 16.1 to 25.6. A
330 very close relationship ($R^2 = 0.98$) was found with extremely high M values (Fig.8d).

331 As noted in Fig.8a-c, close regression slopes implicated that a comprehensive
332 regression model with intermediate M values less than 16 may be achieved. As
333 expected, a promising regression model (the diagram was not shown) between DOC
334 and $a_{CDOM}(275)$ was achieved ($y = 1.269x + 6.42$, $R^2 = 0.909$, N =1171, $p < 0.001$) with
335 pooled dataset shown in Figs.8a-b. Inspired by this idea, the relationship between
336 $a_{CDOM}(275)$ and DOC also examined with pooled data. As shown in Fig.9a, a significant
337 relationship between DOC and $a_{CDOM}(275)$ was obtained with the pooled dataset (N =

1504) collected from different types of inland waters. However, it should be noted that the extremely high DOC samples may advantageously contribute the better performance of the regression model. Thus, regression model excluding these eight samples (DOC > 300 mg/L) was still acceptable (Fig.9b, $R^2 = 0.66$, $p < 0.001$). In addition, regression model with power function was established in decimal logarithms log-log scale (Fig.9c, $R^2 = 0.95$, $p < 0.001$).

[Insert Fig.8 and Fig.9 about here]

4. Discussion

4.1 Variation of water quality parameters

Different water types were sampled across China with different climatic, hydrologic, and land use conditions in various catchment, combined with different anthropogenic intensity, thus the biological and geochemical properties in the water bodies are quite diverse with large range values for each parameters (Table 1). Extremely turbid waters are observed for fresh waters, saline waters and underlying waters covered by ice, which were generally collected in very shallow water bodies in different parts of China. As expected, large variations of Chl-a are observed for both fresh waters and urban waters, and particularly these samples collected in urban waters show large range (1.0-521.1 μg/L). Our investigation also indicates that algal growth is still very active in these ice covered water bodies in Northeast China, which might result from high TN (4.3±5.4mg/L) and TP (0.7±0.6mg/L) concentrations in these waters bodies. It also should be noted that DOC, EC and pH were high in semi-arid or arid climatic regions, which are consistent with previous findings (Curtis and Adams, 1995; Song et al., 2013;

Wen et al., 2016).

4.2 DOC variation with different types of waters

This investigation indicates that lower DOC were encountered with samples collected in rivers from the Tibetan Plateau (Table 2), where the average soil organic matter is lower, thus terrestrial DOC input from the catchment is less (Tian et al., 2008). Generally, low DOC concentrations were found in rivers or streams in the drainage systems in Tibetan Plateau or arid regions in Northwest China where soil contains relative low level of soil organic carbon, but the high DOC concentrations were found in rivers or streams surrounded by forest or wetlands in Northeast China, the similar findings were also reported by Agren et al. (2007, 2011). Further, lower DOC concentration is also measured with ice samples, which is consistent with previous findings (Bezilie et al., 2002; Shao et al., 2016). But relatively high DOC concentration was observed for underlying waters covered by ice in Northeast China due to the condensed effect caused by the DOC discharged from ice formation (Bezilie et al., 2002; Shao et al., 2016; Zhao et al., 2016a). This condensed effect was particularly marked in these shallow water bodies where ice forming remarkably condensed the DOC in the underlying waters (Zhao et al., 2016a). It also should be noted that DOC concentration has a strong connection with hydrological condition and catchment landscape features (Neff et al., 2006; Agren et al., 2007; Lee et al., 2015). Similarly, large DOC variations were observed in saline lakes in different regions (Table 2). Much higher DOC concentrations were found in saline lakes in Qinghai and Hulunbir, while relative low concentrations were observed in Xilinguole Plateau and the Songnen Plain, which is

consistent with previous investigations conducted in the semi-arid or arid regions (Curtis and Adams, 1995; Song et al., 2013; Wen et al., 2016).

4.3 Variation of the relationships between CDOM and DOC

As demonstrated in Fig.3, obvious variation is revealed for the regression slope values between DOC and $a_{CDOM}(275)$. Most of the fresh water bodies are located in East China, where agricultural pollution and anthropogenic discharge have resulted in serious eutrophication (Tong et al., 2017). Phytoplankton degradation may contribute relative large portion of CDOM and DOC in these water bodies (Zhang et al., 2010; Zhou et al., 2016). Comparatively, fresh waters in Northeast and North China revealed larger regression slopes (Table 3). Waters in Northeast China are surrounded by forest, wetlands and grassland and therefore they generally exhibited high proportion of colored fractions of DOC. Further, soils in Northeast China are rich in organic carbon, which may also contribute to high concentration of DOC and CDOM in waters in this region (Jin et al., 2016; Zhao et al., 2016a). Compared with waters in East and South China, waters in Northeast China showed less algal bloom due to low temperature, thus autochthonous CDOM was less presented in waters in Northeast China (Song et al., 2013; Zhao et al., 2016a). As suggested by Brezonik et al. (2015) and Cardille et al. (2013), CDOM in the eutrophic waters or those with very short resident time may show seasonal variation due to algal bloom or hydrological variability, while CDOM in some oligotrophic lakes or those with long resident time may show a stable pattern.

As shown in Fig.3b, smaller regression slope is revealed between DOC and $a_{CDOM}(275)$ for saline waters, indicating less colored portion of DOC was presented in

waters in semi-arid to arid regions, especially for these closed lakes with enhanced photochemical processes (Spencer et al., 2012; Song et al., 2013; Wen et al., 2016). The findings highlighted the difference for the relationship between CDOM and DOC, thus different regression models should be established to accurately estimate DOC in waters through linking with CDOM absorption, particularly for fresh and saline waters that showing different specific absorption coefficients (Song et al., 2013; Cardille et al., 2013; Brezonik et al., 2015).

The current study indicates that CDOM from river and stream waters show higher absorption coefficient, and larger regression slope is revealed (Fig.3c). However, obvious variation for the regression slopes is demonstrated for samples collected in different part of the country (Table 3), which is consistent with the findings from Spencer et al. (2012) and Zhao et al. (2017). Rivers and streams in North, East and South China generally exhibited intermediate values. In addition, water samples in large river generally presents relatively low slope value; streams, especially head water originating from forest and wetland dominated regions show higher regression slope values (e.g., Branches from the Nenjiang and the Songhua River in Table 3), which is consistent with the findings from Spencer et al. (2012). In fact, landscape pattern and soil organic carbon in the catchment are important factors governing the terrestrial DOC and CDOM characteristics in rivers and streams (Wilson and Xenopoulos, 2008; Jaffe et al., 2008; Agren et al., 2011; Lai et al., 2016; Zhao et al., 2017).

DOC concentration is strongly associated with hydrological conditions (Neff et al. 2006; Agren et al. 2007; Yu et al., 2016). The relationships between CDOM and DOC

426 in river and stream waters are very variable due to the hydrological variability and
427 catchment features (Agren et al., 2011; Spencer et al., 2009; 2012; Ward et al., 2013;
428 Lee et al., 2015). As shown in Fig.4, the relationship between river flows and DOC is
429 rather complicated, which is mainly caused by the land use, soil properties, relief, slope,
430 the proportion of wetlands and forest, climate and hydrology of the catchments (Neff
431 et al., 2006; Sobek et al., 2007; Spencer et al., 2012; Zhou et al., 2016), with additional
432 influence by sewage discharge into rivers. For head waters, close relationship between
433 CDOM and DOC is revealed with higher regression slope value (Fig.5a), which is
434 mainly because that the DOC and CDOM were fresh and less disturbed by pollution
435 from anthropogenic activities (Spencer et al., 2012; Shao et al., 2016). Comparatively,
436 loose relationship was revealed for rivers with both point and non-point source
437 pollution that cause the composition and colored fractions of DOC and DOM much
438 varied (Fig.5c). Thereby, both spatial and temporal changes of the relationships
439 between DOC and CDOM were observed, and anthropogenic activities further
440 complicated the relationship.

441 **4.4 Regression models based on CDOM grouping**

442 As observed in Fig.3, the regression slopes (range: 0.33~3.01) for the relationship
443 between DOC and $a_{CDOM}(275)$ varied significantly. The CDOM absorption coefficient
444 is affected by its components and aromacity, thus the M values are used to classify
445 CDOM into different groups, which turns to be an effective approach for improving
446 regression model between DOC and $a_{CDOM}(275)$. Most of the paired data sitting close
447 to the regression line except some scattered ones (Fig. 8a-b). It also should be

highlighted that the fourth group is mainly from saline lakes (samples from embedded diagram in Fig.3b), thus the regression model slope is extremely low. From the regression model with pooled data, it can also be seen that relative accurate regression model for CDOM versus DOC can be achieved with data collected in inland waters at global scale (Sobek et al., 2007), which might be helpful in quantifying DOC through linking with CDOM absorption spectra, and the latter parameter can be estimated from remote sensing data (Zhu et al., 2011; Kuster et al., 2015).

5. Conclusions

Based on the measurement of CDOM absorption spectra and DOC laboratory analysis, we have systematically examined the relationships between CDOM and DOC in various types of waters in China. This investigation showed that CDOM absorption varied significantly. River waters and fresh lake waters exhibited high CDOM absorption values and specific CDOM absorption ($SUVA_{254}$). On the contrast, saline lakes illustrated low $SUVA_{254}$ values due to the long residence time and strong photo-bleaching effects on waters in the semi-arid regions. Influenced by effluents and sewage waters, CDOM from urban water bodies showed much complex absorption characteristics.

The current investigation indicated that the relationships between CDOM absorption and DOC varied remarkably by showing very varied regression slopes in various types of waters. Head river water generally exhibits larger regression slope values, while rivers affected by anthropogenic activities show lower slope values. Saline water generally reveals small regression slope due to the photobleaching effect

in the semi-arid or arid region, combined with longer residence time. The accuracy of regression model between $a_{CDOM}(275)$ and DOC was improved when CDOM absorptions were divided into different sub-groups according to M values. Our finding highlights that remote sensing models for DOC estimation based on the relationship between CDOM and DOC should consider water types or cluster waters into several groups according to their absorption features.

Acknowledgements

The authors would like to thank financial supports from the National Key Research and Development Project (No. 2016YFB0501502), Natural Science Foundation of China (No.41471290), and "One Hundred Talents" Program from Chinese Academy of Sciences granted to Dr. Kaishan Song. Thanks are also extended to all the staff and students for their efforts in field data collection and laboratory analysis, and Dr. Hong Yang to review and polish the English language. Last but not the least, the authors would like to thank the associate editor C. Stamm and three referees for their valuable comments that really help a lot in improving the manuscript.

References

Agren, A., Buffam, I., Jansson, M., Laudon, H., 2007. Importance of seasonality and small streams for the landscape regulation of dissolved organic carbon export. Journal of Geophysical Research, 112: G03003.

Agren, A., Haei, M., Kohler, S.J., Kohler, S.J., Bishop, K., Laudon, H., 2011.

492 Regulation of stream water dissolved organic carbon (DOC) concentrations during
493 snowmelt; the role of discharge, winter climate and memory effects.
494 Biogeosciences, 7, 2901-2913.
495 APHA/AWWA/WEF. 1998. Standard methods for the examination of water and
496 wastewater. Washington, DC: American Public Health Association.
497 Arrigo, K.R., Mock, T., Lizotte, M.P., 2010. Primary producers and sea ice, In *Sea Ice*,
498 edited by D.N. Thomas, and G.S. Dieckmann, pp. 283-326, second ed., Wiley-
499 Blackwell, Oxford, UK.
500 Babin, M., Stramski, D., Ferrari, G. M., Claustre, H., Bricaud, A., Obolensky, G.,
501 Hoepffner, N., 2003. Variations in the light absorption coefficients of
502 phytoplankton, nonalgal particles, and dissolved organic matter in coastal waters
503 around Europe. Journal of Geophysical Research, 108(C7), 3211.
504 Belzile, C., Gibson, J.A.E., Vincent, W.F., 2002. Colored dissolved organic matter and
505 dissolved organic carbon exclusion from lake ice: implications for irradiance
506 transmission and carbon cycling. Limnology and Oceanography, 47(5), 1283–
507 1293.
508 Binding, C.E., Jerome, J.H., Bukata, R.P., Booty, W.G., 2008. Spectral absorption
509 properties of dissolved and particulate matter in Lake Erie. Remote Sensing of
510 Environment, 112(4), 1702-1711.
511 Brezonik, P.L., Olmanson, L.G., Finlay, J.C., Bauer, M.E., 2015. Factors affecting the
512 measurement of CDOM by remote sensing of optically complex inland waters.
513 Remote Sensing of Environment, 157, 199-215.

514 Bricaud, A., Morel, A., Prieur, L., 1981. Absorption by dissolved organic matter of the
515 sea (yellow substance) in the UV and visible domains, Limnology and
516 Oceanography, 26(1), 43– 53.
517 Cardille, J.A., Leguet, J.B., del Giorgio, P., 2013. Remote sensing of lake CDOM using
518 noncontemporaneous field data. Canadian Journal of Remote Sensing, 39, 118–
519 126.
520 Chen, R.F., Bissett, P., Coble, P., Conmy, R., Gardner, G.B., Moran, M.A., Wang, X.C.,
521 Wells, M.L., Whelan, P., Zepp, R.G., 2004. Chromophoric dissolved organic
522 matter (CDOM) source characterization in the Louisiana Bight. Marine Chemistry,
523 89, 257-272.
524 Curtis, P.J., Adams, H.E., 1995. Dissolved organic matter quantity and quality from
525 freshwater and saltwater lakes in east-central Alberta. Biogeochemistry 30, 59–
526 76.
527 De Haan, H., 1993. Solar UV-light penetration and photodegradation of humic
528 substances in peaty lake water. Limnology and Oceanography, 1993, 38, 1072–
529 1076.
530 De Haan, H., De Boer, T., 1987. Applicability of light absorbance and fluorescence as
531 measures of concentration and molecular size of dissolved organic carbon in
532 humic Lake Tjeukemeer. Water Research, 21, 731–734.
533 Fichot, C.G., Benner, R., 2011. A novel method to estimate DOC concentrations from
534 CDOM absorption coefficients in coastal waters. Geophysical Research Letter,
535 38, L03610.

536 Findlay, S.E.G., Sinsbaugh, R.L., 2003. Aquatic Ecosystems Interactivity of Dissolved
537 Organic Matter. Academic Press, San Diego, CA, USA.
538 Gonnelli, M., Vestri, S., Santinelli, C., 2013. Chromophoric dissolved organic matter
539 and microbial enzymatic activity. A biophysical approach to understand the marine
540 carbon cycle. Biophysical Chemistry, 182, 79-85.
541 Helms, J.R., Stubbins, A., Ritchie, J.D., Minor, E.C., Kieber, D.J., Mopper, K., 2008.
542 Absorption spectral slopes and slope ratios as indicators of molecular weight,
543 source, and photobleaching of chromophoric dissolved organic matter. Limnology
544 and Oceanography, 53, 955–969.
545 Huang, C.C., Li, Y.M., Yang, H., Li, J.S., Chen, X., Sun, D.Y., Le, C.F., Zou, J., Xu,
546 L.J., 2014. Assessment of water constituents in highly turbid productive water by
547 optimization bio-optical retrieval model after optical classification. Journal of
548 Hydrology, 519, 1572–1583.
549 Jaffé, R., McKnight, D., Maie, N., Cory, R., McDowell, W.H., Campbell, J.L., 2008.
550 Spatial and temporal variations in DOM composition in ecosystems: The
551 importance of long-term monitoring of optical properties. Journal of Geophysical
552 Research, 113, G04032.
553 Jeffrey, S.W., Humphrey G.F., 1975. New spectrophotometric equations for
554 determining chlorophylls *a, b,* c_1, and c_2 in higher plants, algae and natural
555 phytoplankton. Biochemie und Physiologie der Pflanzen, 167(2), 191–194.
556 Jin, X.L., Du, J., Liu, H.J., Wang, Z.M., Song, K.S., 2016. Remote estimation of soil
557 organic matter content in the Sanjiang Plain, Northeast China: The optimal band

558 algorithm versus the GRA-ANN model. Agricultural and Forest Meteorology, 218,
559 250–260.
560 Kowalczuk, P., Zablocka, M., Sagan, S., Kulinski, K., 2010. Fluorescence measured in
561 situ as a proxy of CDOM absorption and DOC concentration in the Baltic Sea.
562 Oceanologia, 52(3), 431–471.
563 Kutser, T., Verpoorter, C., Paavel, B., Tranvik, L.J., 2015. Estimating lake carbon
564 fractions from remote sensing data. Remote Sensing of Environment, 157, 138–
565 146.
566 Lai, L., Huang, X., Yang, H., Chuai, X., Zhang, M., Zhong, T., Chen, Z., Chen, Y.,
567 Wang, X., Thompson, J.R., 2016. Carbon emissions from land-use change and
568 management in China between 1990 and 2010. Science Advances, 2(11),
569 e1601063.
570 Le, C.F., Hu, C.M., Cannizzaro, J., Duan, H.T., 2013. Long-term distribution patterns
571 of remotely sensed water quality parameters in Chesapeake Bay. Estuarine,
572 Coastal and Shelf Science, 128(10), 93–103.
573 Lee, E.J., Yoo, G.Y., Jeong, Y., Kim, K.U., Park, J.H., Oh, N.H., 2015. Comparison of
574 UV–VIS and FDOM sensors for in situ monitoring of stream DOC concentrations.
575 Biogeosciences, 12, 3109–3118.
576 Lee, Z.P., Carder, K.L., Arnone, R.A., 2002. Deriving inherent optical properties from
577 water color: A multiband quasi-analytical algorithm for optically deep waters.
578 Applied Optics, 41(27), 5755–577.
579 Miller, W.L., Zepp, R.G., 1995. Photochemical production of dissolved inorganic

carbon from terrestrial organic matter: Significance to the oceanic organic carbon cycle. Geophysical Research Letter, 22 (4), 417–420.

Neff, J.C., Finlay, J.C., Zimov, S.A., Davydov, S.P., Carrasco, J.J., Schuur, E.A.G., Davydova, A.I., 2006. Seasonal changes in the age and structure of dissolved organic carbon in Siberian rivers and streams. Geophysical Research Letter, 33, L23401.

Pekel, J.F., Cottam, A., Gorelick, N., Belward, A.S., 2016. High-resolution mapping of global surface water and its long-term changes. Nature, 540, 417–422.

Raymond, P. A., Hartmann, J., Lauerwarld, R., et al., 2013. Global carbon dioxide emissions from inland waters. Nature, 503(7476), 355–359.

Reche, I., Pace, M., Cole, J.J., 1999. Relationship of trophic and chemical conditions to photobleaching of dissolved organic matter in lake ecosystems. Biogeochemistry, 44, 529–280.

Shao, T.T., Song, K.S., Du, J., Zhao, Y., Ding, Z., Guan, Y., Liu, L., Zhang, B., 2016. Seasonal variations of CDOM optical properties in rivers across the Liaohe Delta. Wetlands, 36 (suppl.1): 181–192.

Shi, K., Li, Y., Li, L., et al., 2013. Remote chlorophyll-a estimates for inland waters based on a cluster-based classification. Science of the Total Environment, 444, 1–15.

Spencer, R.G.M., Stubbins, A., Hernes, P.J., Baker, A., Mopper, K., Aufdenkampe, A.K., Dyda, R.Y., Mwamba, V.L., Mangangu, A.M., Wabakanghanzi, J.N., Six, J., 2009. Photochemical degradation of dissolved organic matter and dissolved

602 ligninphenols from the Congo River. Journal of Geophysical Research, 114,
603 G03010.
604 Spencer, R.G.M., Butler, K.D., Aiken, G.R., 2012. Dissolved organic carbon and
605 chromophoric dissolved organic matter properties of rivers in the USA. Journal
606 of Geophysical Research, 117, G03001.
607 Sobek, S., Tranvik, L.J., Prairie, Y.T., Kortelainen, P., Cole, J.J., 2007. Patterns and
608 regulation of dissolved organic carbon: An analysis of 7,500 widely distributed
609 lakes. Limnology and Oceanography 52, 1208–1219.
610 Song, K.S., Zang, S.Y., Zhao, Y., Li, L., Du, J., Zhang, N.N., Wang, X.D., Shao, T.T.,
611 Liu, L., Guan, Y., 2013. Spatiotemporal characterization of dissolved Carbon for
612 inland waters in semi-humid/semiarid region, China. Hydrology and Earth
613 System Science, 17, 4269–4281.
614 Stedmon, C.A., Thomas, D.N., Papadimitriou, S., Granskog, M.A., Dieckmann, G.S.
615 2011. Using fluorescence to characterize dissolved organic matter in Antarctic
616 sea ice brines. Journal of Geophysical Research, 116, G03027.
617 Tian, Y.Q., Ouyang, H., Xu, X.L., Song, M.H., Zhou, C.P., 2008. Distribution
618 characteristics of soil organic carbon storage and density on the Qinghai-Tibet
619 Plateau. Acta Pedologica Sinica, 45(5), 933–942. (In Chinese with English
620 abstract).
621 Tong, Y.D., Zhang, W., Wang, X.J., et al., 2017. Decline in Chinese lake phosphorus
622 concentration accompanied by shift in sources since 2006. Nature Geoscience,
623 10(7), 507–511.

624 Tranvik, L.J., Downing, J.A., Cotner, J.B., et al., 2009. Lakes and reservoirs as
625 regulators of carbon cycling and climate. Limnology and Oceanography, 54(6),
626 2298–2314.
627 Vantrepotte, V., Loisel, H., Dessailly, D., et al., 2012. Optical classification of
628 contrasted coastal waters. Remote Sensing of Environment, 123, 306–323.
629 Verpoorter, C., Kutser, T., Seekell, D.A., Tranvik, L.J., 2014. A global inventory of
630 lakes based on high-resolutionsatellite imagery. Geophysical Research Letter, 41,
631 6396–6402.
632 Vodacek, A., Blough, N.V., Degrandpre, M.D., Peltzer, E.T., Nelson, R.K., 1997.
633 Seasonal variation of CDOM and DOC in the Middle Atlantic Bight: terrestrial
634 inputs and photooxidation. Limnology and Oceanography, 42, 674–686.
635 Ward Jr, J.H., 1963. Hierarchical grouping to optimize an objective function. Journal of
636 the American Statistical Association, 58(301), 236–244.
637 Ward, N.D., Keil, R.G., Medeiros, P.M., Brito, D.C., Cunha, A.C., Dittmar, T., Yager,
638 P.L., Krusche, A.V. and Richey, J.E., 2013. Degradation of terrestrially derived
639 macromolecules in the Amazon River. Nature Geoscience, 6(7), 530–533.
640 Weishaar, J.L., Aiken, G.R., Bergamaschi, B.A., Fram, M.S., Fugii, R., Mopper, K.,
641 2003. Evaluation of specific ultraviolet absorbance as an indicator of the chemical
642 composition and reactivity of dissolved organic carbon. Environmental Science
643 and Technology, 37, 4702–4708.
644 Wen, Z.D., Song, K.S., Zhao, Y., Du, J., Ma, J.H., 2016. Influence of environmental
645 factors on spectral characteristic of chromophoric dissolved organic matter

(CDOM) in Inner Mongolia Plateau, China. Hydrology and Earth System Sciences, 20, 787–801.

Williamson, C.E., Rose, K.C., 2010. When UV meets fresh water. Science, 329, 637–639.

Wilson, H., Xenopoulos, M.A., 2008. Ecosystem and seasonal control of stream dissolved organic carbon along a gradient of land use. Ecosystems 11, 555–568.

Yang, H., Andersen, T., Dörsch, P.,Tominaga, K., Thrane, J.-E., Hessen, D. O., 2015. Greenhouse gas metabolism in Nordic boreal lakes. Biogeochemistry, 126, 211–225.

Yang, H., Xie, P., Ni, L., Flower, R. J., 2012. Pollution in the Yangtze. Science, 337, (6093), 410-410.

Yu, Q., Tian, Y, Q., Chen, R.F., Liu, A., Gardner, G.B., Zhu, W.N., 2010. Functional linear analysis of in situ hyperspectral data for assessing CDOM in rivers. Photogrammetric Engineering & Remote Sensing, 76(10), 1147–1158.

Yu, X.L., Shen, F., Liu, Y.Y., 2016. Light absorption properties of CDOM in the Changjiang (Yangtze) estuarine and coastal waters: An alternative approach for DOC estimation. Estuarine, Coastal and Shelf Science, 181, 302–311.

Zhang, Y.L., Zhang, E.L., Yin, Y., Van Dijk, M.A., Feng, L.Q., Shi, Z.Q., Liu, M.L., Qin, B.Q., 2010. Characteristics and sources of chromophoric dissolved organic matter in lakes of the Yungui Plateau, China, differing in trophic state and altitude. Limnology and Oceanography, 55(6), 2645–2659.

Zhao, Y., Song, K.S., Wen, Z.D., Li, L., Zang, S.Y., Shao, T.T., Li, S.J., Du, J., 2016a.

668 Seasonal characterization of CDOM for lakes in semiarid regions of Northeast
669 China using excitation–emission matrix fluorescence and parallel factor analysis
670 (EEM–PARAFAC). Biogeosciences, 13, 1635–1645.
671 Zhao, Y., Song, K.S., Li, S.J., Ma, J.H., Wen, Z.D., 2016b. Characterization of CDOM
672 from urban waters in Northern-Northeastern China using excitation-emission
673 matrix fluorescence and parallel factor analysis. Environmental Science and
674 Pollution Research, 23, 15381–15394.
675 Zhao, Y., Song, K.S., Shang, Y. X., Shao, T. T., Wen, Z.D., Lv, L.L., 2017.
676 Characterization of CDOM of river waters in China using fluorescence excitation-
677 emission matrix and regional integration techniques. Journal of Geophysical
678 Research, Biogeoscience, DOI: 10.1002/2017JG003820.
679 Zhou Y., Zhang Y., Jeppesen E., Murphy K.R., Shi K., Liu M., Liu X., Zhu G. Inflow
680 rate-driven changes in the composition and dynamics of chromophoric dissolved
681 organic matter in a large drinking water lake. Water Research, 2016, 100, 211-221.
682 Zhu, W., Yu, Q., Tian, Y. Q., Chen, R.F., Gardner, G.B., 2011. Estimation of
683 chromophoric dissolved organic matter in the Mississippi and Atchafalaya river
684 plume regions using above-surface hyperspectral remote sensing. Journal of
685 Geophysical Research: Oceans (1978–2012), 116(C2), C02011.
686 Zhu, W.N., Yu, Q., Tian, Y. Q., et al., 2014. An assessment of remote sensing algorithms
687 for colored dissolved organic matter in complex freshwater environments. Remote
688 Sensing of Environment, 140, 766-778.

Figures

Fig.1. The potential regulating factors that influence the relationship between CDOM and DOC. Note, hydrological feature includes flow discharge, drainage area, catchment landscape, river level, and inflow or outflow regions.

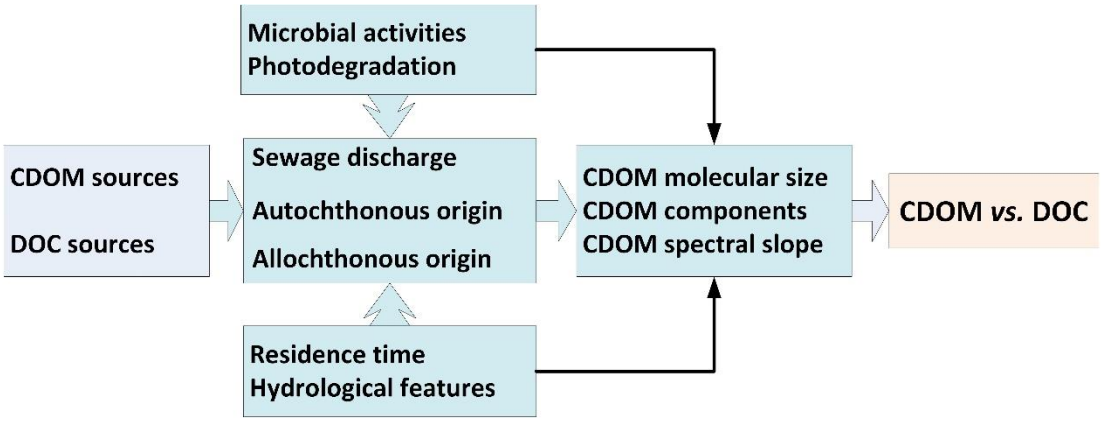

Fig.2. Water types and sample distributions across the mainland China. The dash line shows the boundary of some typical geographic units (i.e., Tibet Plateau, Songnen Plain, and Hulun Buir Plateau).

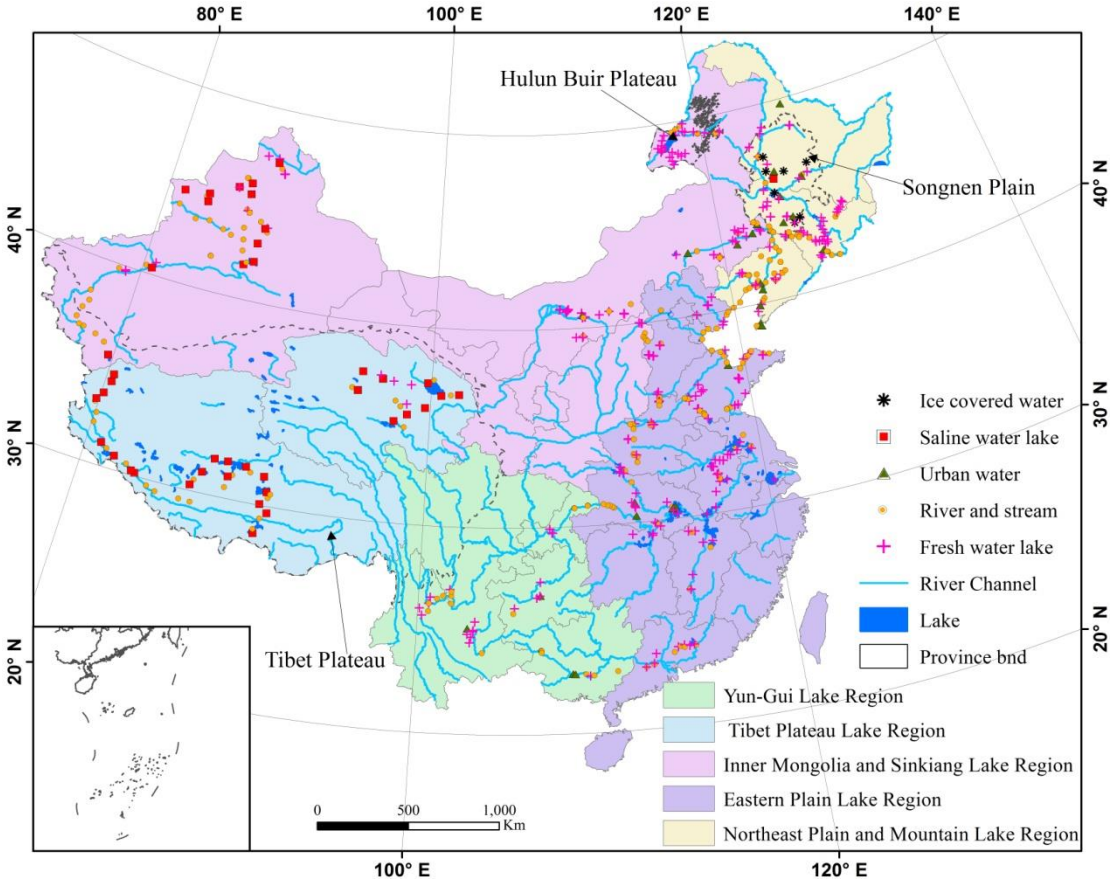

735 Fig.3. Relationship between DOC and $a_{CDOM}(275)$ in different types of inland waters,
736 (a) fresh water lakes, (b) saline water lakes, (c) river and stream waters, (d) urban waters,
737 (e) ice covered lake underlying waters, and (f) ice melting lake waters.

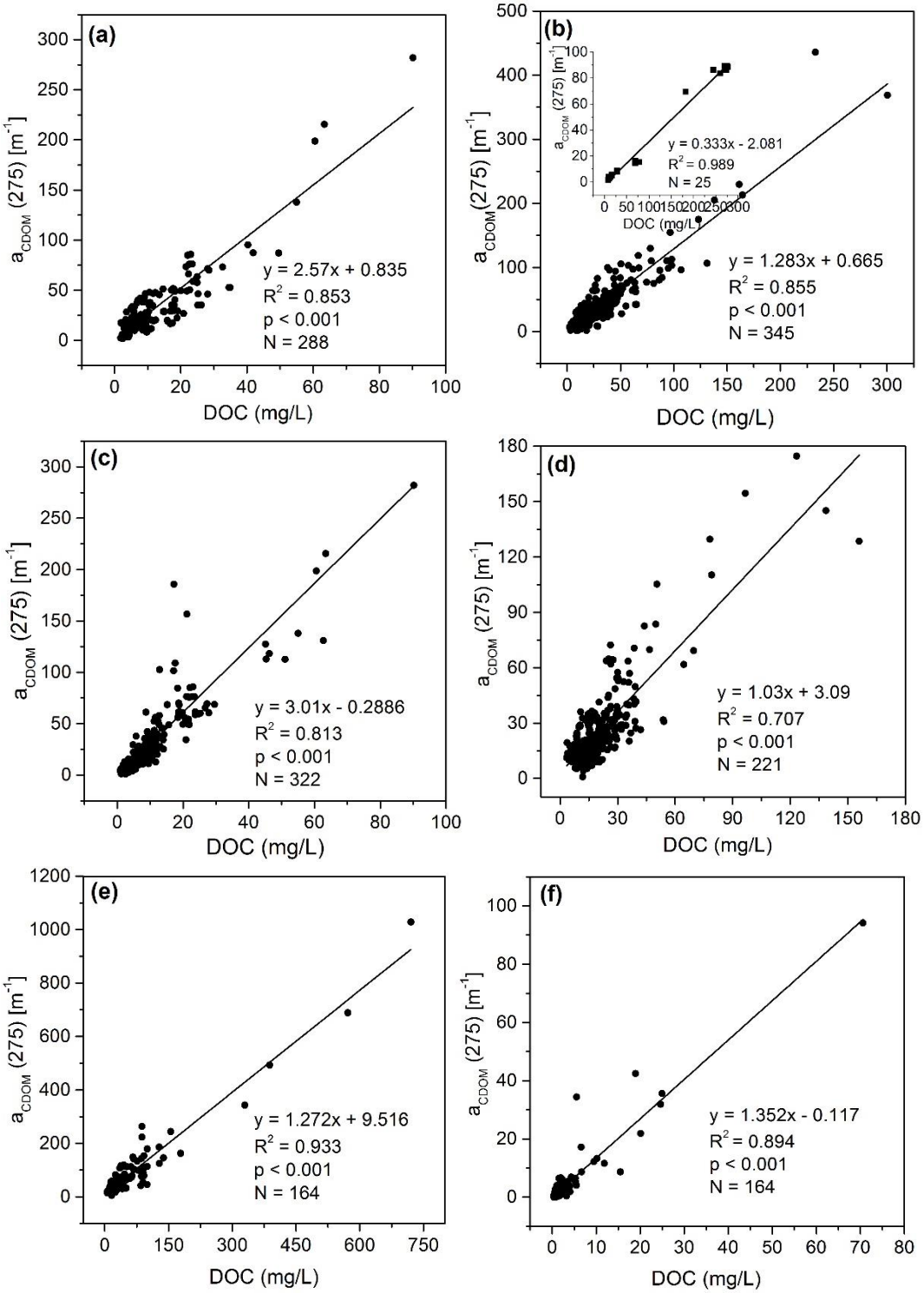

738
739
740
741
742
743

Fig.4. Concurrent flow dynamics for three rivers in Northeast China and the corresponding DOC and CDOM variations in 2015; (a) the Yalu River near Changbai County, (b) the Hunjiang River with DOC and CDOM sampled at Baishan City, while the river flow gauge station is near the Tonghua City, (c) the Songhua River at Harbin City.

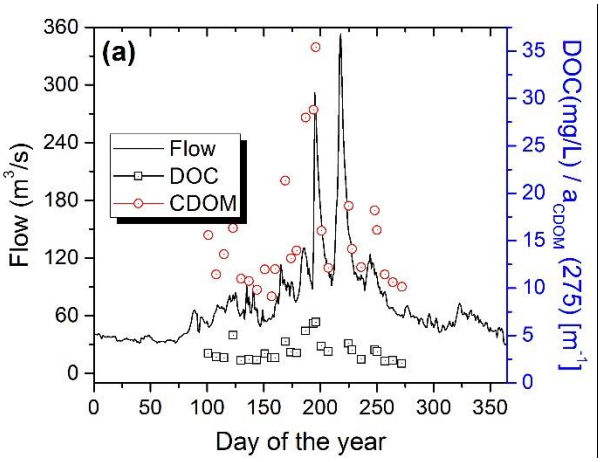

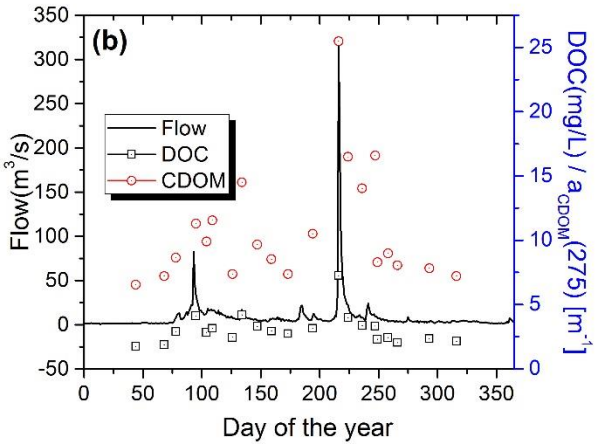

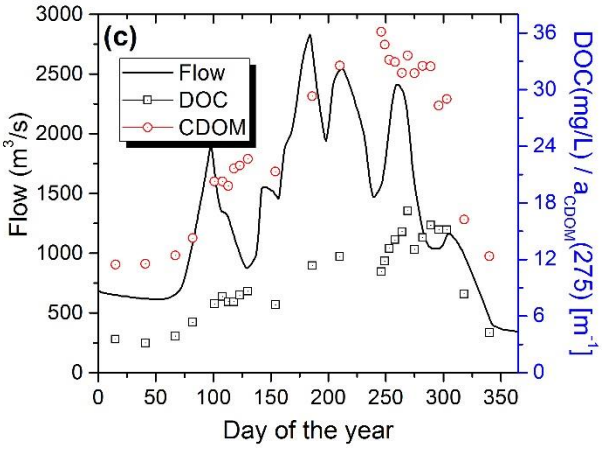

Fig.5. The relationships between $a_{CDOM}(275)$ and DOC at sections across (a) the Yalu River, (b) the Hunjiang River, and (c) the Songhua River. The samples were collected at each station at about one week or around ten days in ice free season in 2015.

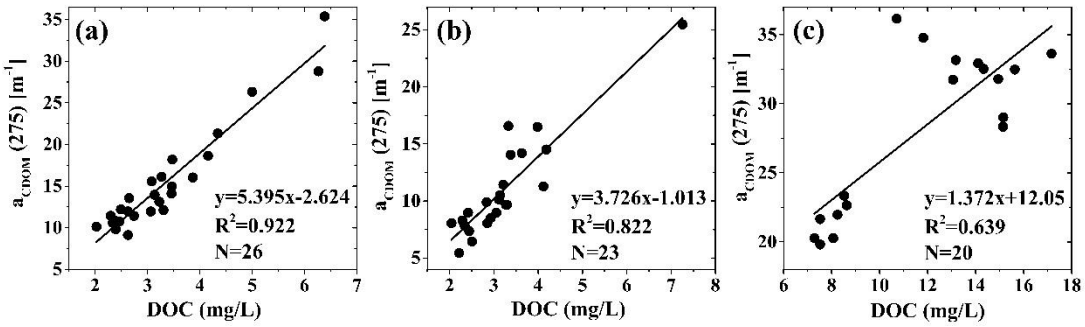

780 Fig.6. Relationship between DOC and $a_{CDOM}(440)$ in different types of inland waters,
781 (a) fresh water lakes, (b) saline water lakes, (c) river and stream waters, (d) urban waters,
782 (e) ice covered lake underlying waters, and (f) ice melting waters.

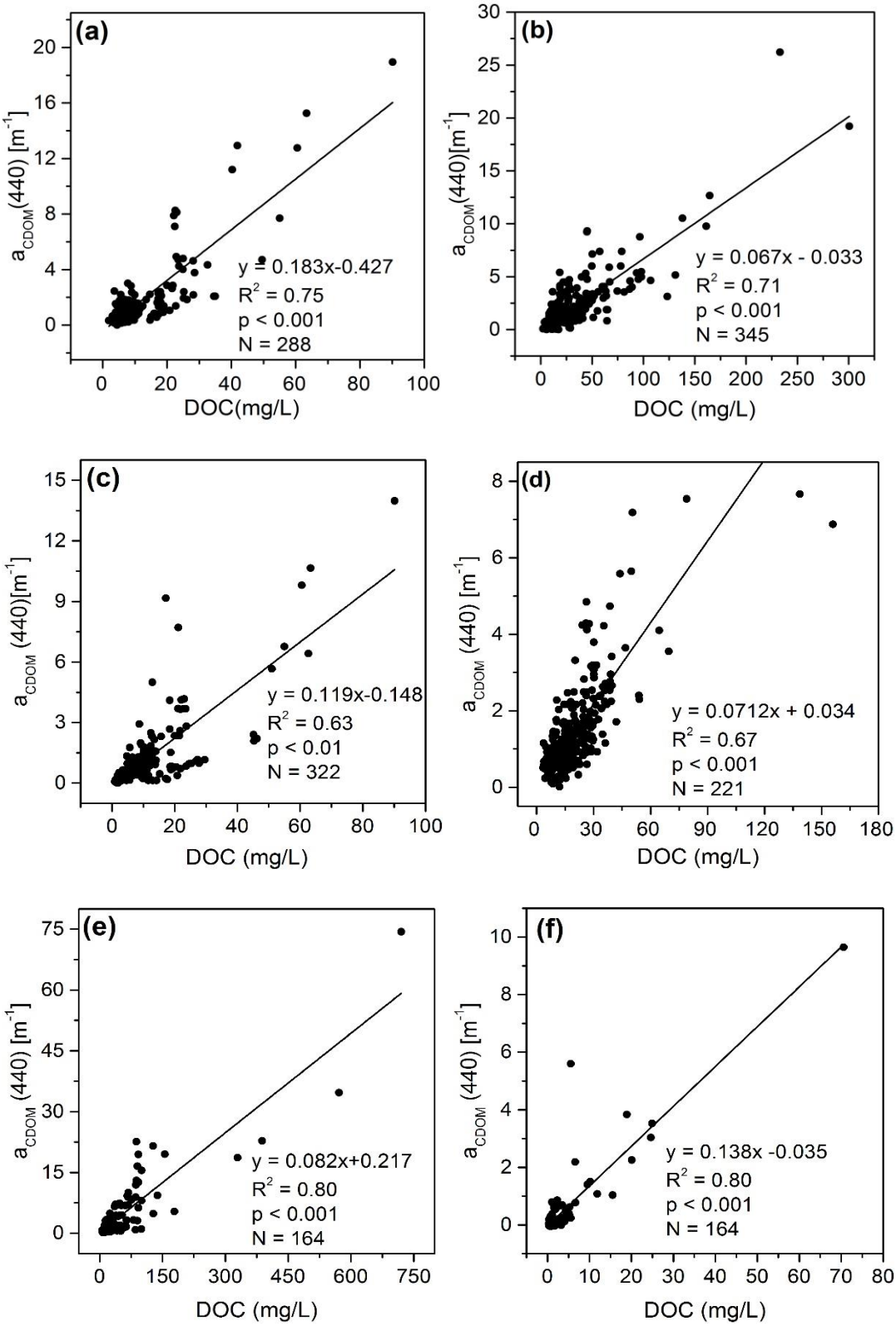

783
784
785
786

Fig.7. Comparison of (a) $SUVA_{254}$, and (b) M values ($a_{CDOM}(250)$ / $a_{CDOM}(365)$) in various types of inland waters. FW, fresh lake water; SW, saline lake water, RW, river or stream water; UW, urban water; WW, ice covered waters from Northeast China; IMW, ice melt waters from Northeast China.

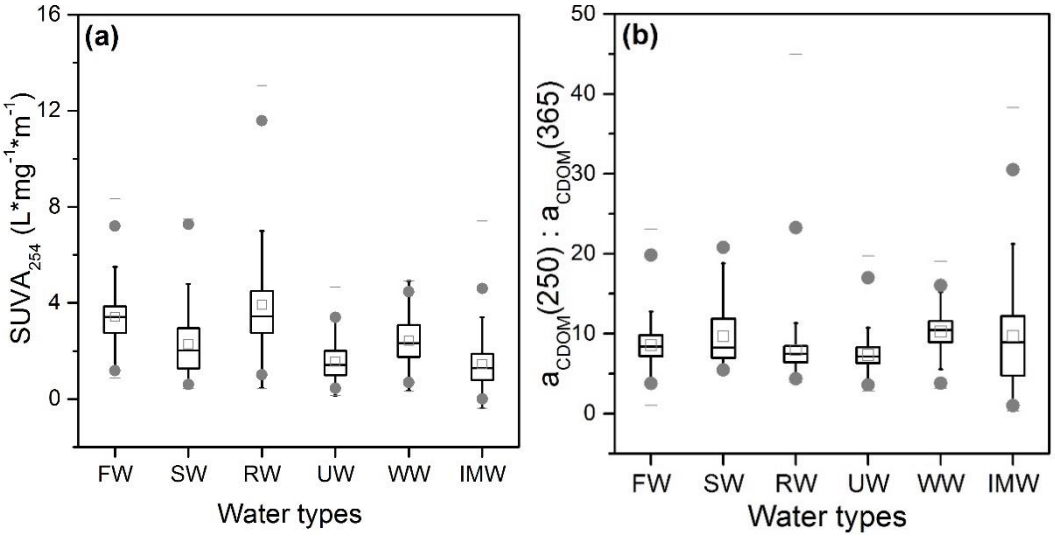

Fig.8. Relationship between DOC and $a_{CDOM}275$ sorted by M ($a_{CDOM}(250)/a_{CDOM}(365)$) values, (a) M <8.5, (b) 8.5< M<16.1, (c) 16.1< M< 25.6, and (d) 25.6< M< 68.0.

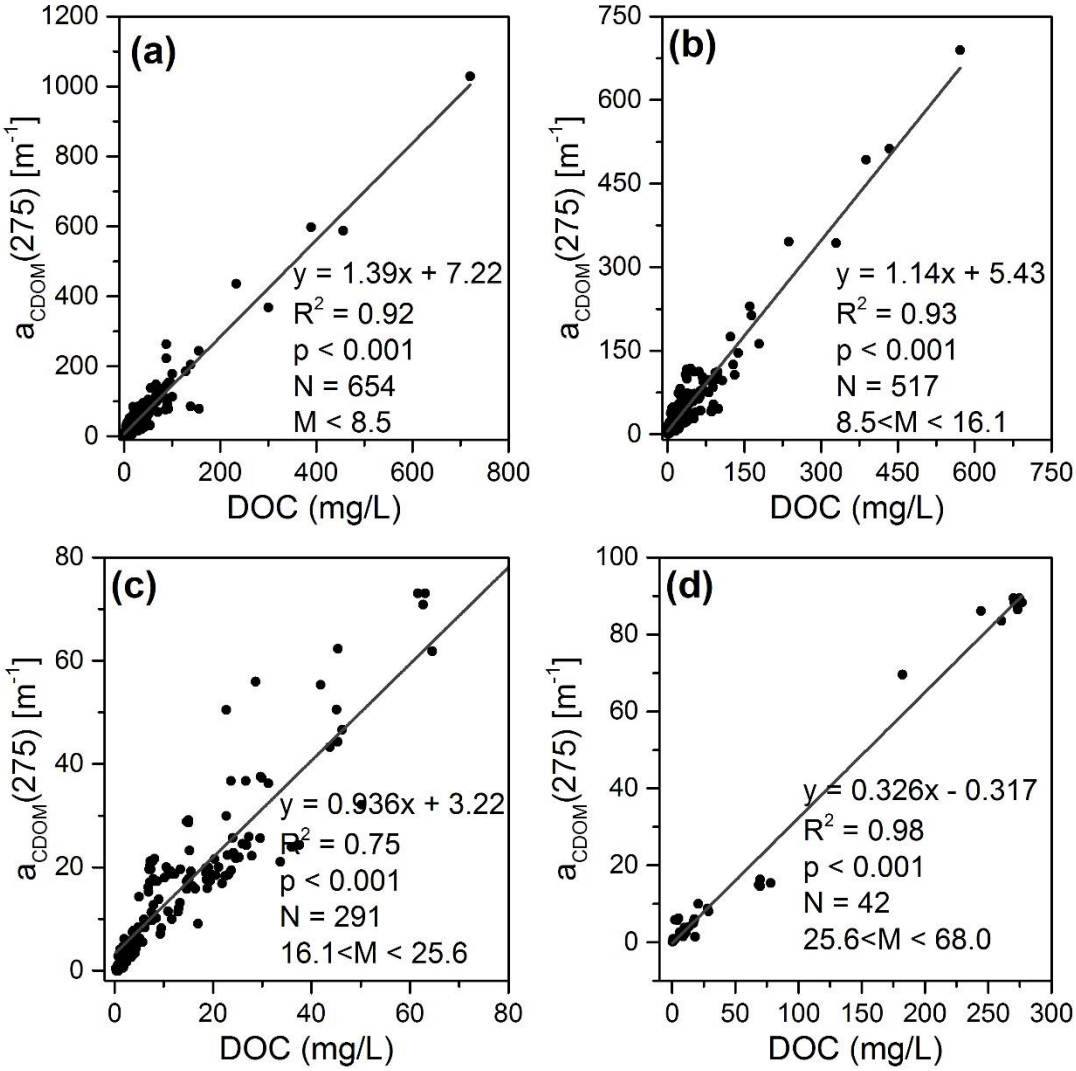

Fig.9. the relationships between $a_{CDOM}(275)$ and DOC concentrations. (a) regression model with pooled dataset; (b) regression model with DOC concentration less than 300 mg/L; (c) regression model with power fitting function based on log-log scale.

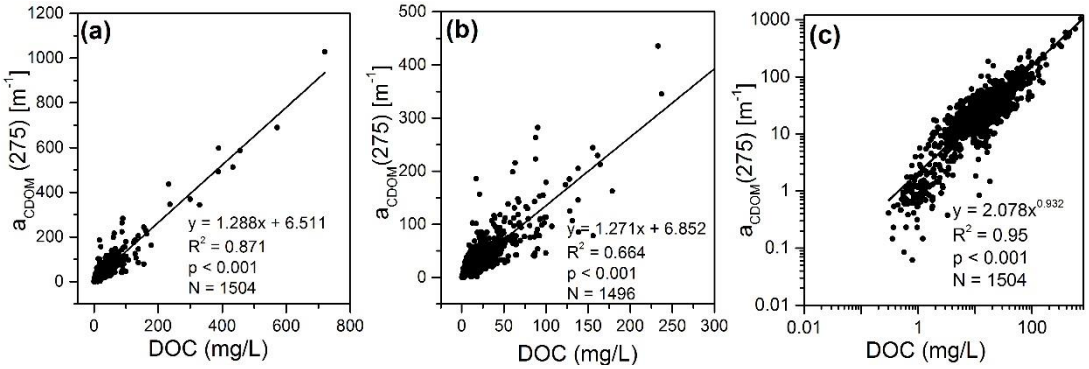

Tables

Table 1. Water quality in different types of waters, DOC, dissolved organic carbon; EC, electrical conductivity; TP, total phosphorus; TN, total nitrogen; TSM, total suspended matter; Chl-a, chlorophyll-a concentration.

		DOC (mg/L)	EC µs/cm	pH	TP (mg/L)	TN (mg/L)	TSM (mg/L)	Chl-a (µg/L)
FW	Mean	10.2	434.0	8.2	0.5	1.6	67.8	78.5
	Range	1.9-90.2	72.7-1181.5	6.9-9.3	0.01-10.4	0.001-9.5	0-1615	1.4-338.5
SW	Mean	27.3	4109.4	8.6	0.4	1.4	115.7	9.0
	Range	2.3-300.6	1067-41000	7.1-11.4	0.01-6.3	0.6-11.0	1.4-2188	0-113.7
RW	Mean	8.3	10489.1	7.8-9.5	-	-	-	-
	Range	0.9-90.2	3.7-1000	8.6	-	-	-	-
UW	Mean	19.44	525.4	8.0	3.4	3.5	50.5	38.9
	Range	3.5-123.3	28.6-1525	6.4-9.2	0.03-32.4	0.04-41.9	1-688	1.0-521.1
WW	Mean	67.0	1387.6	8.1	0.7	4.3	181.5	7.3
	Range	7.3-720	139-15080	7.0-9.7	0.1-4.8	0.5-48	9.0-2174	1.0-159.4
IMW	Mean	6.7	242.8	8.3	0.19	1.1	17.4	1.1
	Range	0.3-76.5	1.5-4350	6.7-10	0.02-2.9	0.3-8.6	0.3-254.6	0.28-5.8

Note: FW, fresh water lake; SW, saline water lake, RW, river or stream water; UW, urban water; WW, ice covered winter water from Northeast China; IMW, ice melt water from Northeast China.

Table 2. Descriptive statistics of dissolved organic carbon (DOC) and $a_{CDOM}(440)$ in various types of waters.

Type	Region	DOC (mg/L)				$a_{CDOM}(440)$ [m^{-1}]			
		Min	Max	Mean	S.D	Min	Max	Mean	S.D
River	Liaohe	3.6	48.2	14.3	9.49	0.46	3.68	0.92	0.58
	Qinghai	1.2	8.5	4.4	1.96	0.13	2.11	0.54	0.63
	Inner Mongolia	16.9	90.2	40.4	24.84	0.32	7.46	1.03	2.11
	Songhua	0.9	21.1	8.1	4.96	0.32	18.93	3.2	4.19
Saline	Qinghai	1.7	130.9	67.9	56.7	0.13	0.86	0.36	0.23
	Hulunbir	8.4	300.6	68.5	69.2	0.82	26.21	4.41	4.45
	Xilinguole	3.74	45.4	14.2	8.8	0.36	4.7	1.34	0.88
	Songnen	3.6	32.6	16.4	7.4	0.46	33.80	2.4	3.78

908 Table 3. Fitting equations for DOC against $a_{CDOM}(275)$ in different types of waters
909 except ice covered lake underlying water and ice melting waters.

Water types	Region or Basin	Equations	R^2	N
Freshwater lakes	Northeast Lake Zone	y = 3.13x-3.438	0.87	102
	North Lake Zone	y = 2.16x-1.279	0.90	63
	East Lake Zone	y = 1.98x+7.813	0.66	69
	Yungui Lake Zone	y = 1.295x-44.56	0.71	54
Saline lakes	Songnen Plain	y = 2.383x+1.101	0.92	159
	East Mongolia	y = 1.791x+8.560	0.67	57
	West Mongolia	y = 1.133x+3.900	0.81	46
	Tibetan Plateau	y = 0.864x+2.255	0.84	83
Rivers or streams	Branch of the Nenjiang River	y = 7.655x-42.64	0.81	33
	Songhua River stem	y = 3.759x-6.618	0.71	29
	Branch of Songhua River	y = 8.496x-12.14	0.98	33
	Liao River Autumn 2012	y = 1.099x+3.900	0.80	38
	Liao River Autumn 2013	y = 1.073x-4.157	0.88	28
	Liao River Spring 2013	y = 2.262x-10.32	0.85	25
	Rivers from North China	y = 3.154x-1.207	0.87	48
	Rivers from East China	y = 3.037x-2.585	0.88	47
	Rivers from Tibetan	y = 2.345x+2.375	0.87	41
Urban waters	Waters from Changchun	y = 2.471x-2.231	0.54	48
	Waters from Harbin	y = 1.413x-4.521	0.67	31
	Waters from Beijing	y = 0.874x+11.12	0.63	27
	Waters from Tianjin	y = 0.994x + 7.368	0.57	23

910
911
912